NATIONAL ADVISORY COMMITTEE FOR AERONAUTICS

TECHNICAL NOTE 3697

FLIGHT TESTS AT SUPERSONIC SPEEDS TO DETERMINE THE EFFECT OF TAPER ON THE ZERO-LIFT DRAG OF SWEPTBACK LOW-ASPECT-RATIO WINGS

By Murray Pittel

Langley Aeronautical Laboratory
Langley Field, Va.

Washington
June 1956

NATIONAL ADVISORY COMMITTEE FOR AERONAUTICS

TECHNICAL NOTE 3697

FLIGHT TESTS AT SUPERSONIC SPEEDS TO DETERMINE THE EFFECT OF TAPER ON THE ZERO-LIFT DRAG OF SWEPTBACK LOW-ASPECT-RATIO WINGS

By Murray Pittel[1]

SUMMARY

Rocket-powered models have been flown to provide an experimental comparison with linearized theoretical calculations for zero-lift drag of sweptback tapered wings having thin, symmetrical, double-wedge airfoil sections. The range of the experimental data is from a Mach number M of 1.0 to 1.8, and theoretical comparisons are made for the test range above M = 1.2.

The linearized theory compared very favorably with the experimental results over most of the test range. For a given thickness and aspect ratio, taper generally increased the wing drag at low supersonic speeds but reduced the drag at higher speeds. For a given thickness and taper ratio, the wings of aspect ratio 4 had less drag below $M \approx 1.2$, but greater drag above $M \approx 1.2$, than the wings of aspect ratio 2.

INTRODUCTION

Airfoil theory for supersonic wave drag of thin, symmetrical, double-wedge sections (refs. 1 and 2) has indicated the effect of taper and aspect ratio on wing drag. The purpose of the present investigation was to provide experimental correlation for the theory of references 1 and 2.

The wing configurations had constant sweep of 50° of the 0.5 chord line and taper ratios of 0, 1/3, and 2/3 for aspect ratios of 2 and 4. The airfoils were constant 6-percent-thick double-wedge sections in order that a valid comparison could be made with the theory.

---

[1]Supersedes recently declassified NACA Research Memorandum L50F30a by Murray Pittel, 1950.

The flight tests were made by using the rocket-powered-model technique at the Pilotless Aircraft Research Station at Wallops Island, Va. and covered a range of Mach number from 1.0 to 1.8 corresponding to an average Reynolds number range from approximately 5×10^6 to 10×10^6 based on the mean aerodynamic chord of the exposed wing surfaces. The wing drag presented in this paper includes mutual interference effects between wing and body.

SYMBOLS

C_{D_T}	total-drag coefficient of test vehicle based on an exposed wing area of 200 square inches
C_{D_W}	wing-drag coefficient based on an exposed wing area of 200 square inches
c_t	tip chord measured in free-stream direction, inches
c_r	root chord measured at wing-fuselage juncture, inches
c_t/c_r	taper ratio
S	wing area, square inches
V	velocity of test vehicle
c	sonic velocity, feet per second
M	Mach number (V/c)
g	acceleration of gravity, 32.17 feet per second^2
ρ	mass density of air, slugs per cubic foot
a	acceleration of model, feet per second^2
W	weight of model, powder expended, pounds
γ	angle of launch, degrees

CONFIGURATION AND TESTS

Configuration.- The models were so constructed as to have wings with taper ratios of 0, 1/3, and 2/3 for aspect ratios, based on the exposed surface, of 2.0 and 4.0 with the wing maximum-thickness line swept back 50° (figs. 1(a) and 1(b)). Although the aspect ratio based on the exposed surfaces has been held constant for each of the families of taper ratio, the total aspect ratio (including the section of wing covered by the body) is different for each of the test models. The

table below lists the values of total aspect ratio for each model, but further reference to aspect ratio in this report refers only to the values for the exposed surfaces:

Aspect ratio based on exposed surface	Taper ratio	Total aspect ratio
2.0	0	2.00
	1/3	2.22
	2/3	2.34
4.0	0	4.00
	1/3	4.30
	2/3	4.50

The free-stream profile was a double-wedge section of 6-percent-thickness ratio. The wings were mounted with zero incidence angle on a standard body (fig. 2(a)) so that the one-quarter point of the mean aerodynamic chord lay at station 34.5 along the body. Photographs of the test vehicles are shown in figures 2(b) and 2(c).

The standard body was an all-wood shell with four metal stabilizing fins spaced equally around the body (fig. 2(a)). The body was 5 inches in diameter and about 5 feet long. It consisted of a sharp nose of nearly circular arc profile having a fineness ratio of 3.5 and a hollow cylindrical afterbody. The stabilizing fins were tapered in plan form and had rectangular sections with rounded leading edges swept back 45° and square trailing edges. The wings, which were placed on the standard body, were indexed 45° to the fins. The wings were fabricated of magnesium and mounted by means of support brackets to the sustainer motor case which was enclosed in the hollow fuselage.

The models were propelled by means of a two-stage system wherein the booster was a 5-inch, high-velocity, aircraft rocket motor having stabilizing fins of 1600-square-inch total exposed area. The model sustainer motor was a 3.25-inch Mark 7 aircraft rocket.

Tests.- The flight tests were conducted at the Pilotless Aircraft Research Station at Wallops Island, Va.

Two models of each winged configuration were flown and data were obtained for all models except for one winged model of taper ratio 2/3, aspect ratio 2.0. Six models of the standard body wingless configuration were flown from which data were obtained over a Mach number range of 0.8 to 2.1.

The experimental data were obtained by launching the model at an angle of 70° to the horizontal and by determining its velocity along a nearly straight-line flight path. The velocity determination is made possible by a Doppler velocimeter located at the point of launching. The CW Doppler velocimeter radar unit is located at the launching site and consists essentially of two parabolic reflectors each with an antenna: one to transmit continuous-wave signals of known frequency along a conical beam and the other to receive them after they are reflected off the moving vehicle. The beat frequency between the transmitted and received signals is a function of the velocity of the vehicle and is recorded photographically. The flight velocities are then ascertained from these film records. Acceleration is obtained from a numerical differentiation of the velocity-time history of the model's flight and drag coefficient is reduced from the following equation:

$$C_D = \frac{-2W(a + g \sin \gamma)}{g\rho SV^2}$$

The variations of temperature and static pressure with altitude used in calculating the drag coefficient and Mach number of the models were obtained from radiosonde observations made at the time of firing.

The probable inaccuracy in the values of wing-drag coefficient is approximately ±0.002. The Mach number is believed to be correct to within ±0.01. No data have been presented below a Mach number of 1.0 because of the unknown curvature in the flight paths of the test models during the last several seconds of measurable flight.

RESULTS AND DISCUSSION

The variation in Reynolds number with Mach number for each of the test configurations is given for the range of the tests in figure 3. The Reynolds number has been based on the mean aerodynamic chord of the exposed wing surfaces.

The data obtained from the flight tests of the winged models are presented in figures 4(a), 4(b), and 4(c) as total-drag coefficient, based on an exposed wing area of 1.389 square feet, plotted against Mach number. The symbols used represent calculated test points for each model of each configuration flown. The total-drag-coefficient data plotted against Mach number for the basic wingless body are shown in figure 5. The drag-coefficient values of the basic wingless body are based on a wing area of 1.389 square feet for comparison with the drag coefficients of the winged bodies.

Wing-drag coefficients obtained as the difference in total-drag coefficient between a winged and wingless configuration are plotted against Mach number in figure 6 for a comparison of wings of three taper ratios. These data include the mutual interference between wing and body. For each of the two aspect ratios tested the results showed that, from $M \approx 1.0$ to $M \approx 1.3$, the more highly tapered wings had the greatest drag but had the least drag above $M \approx 1.3$.

In figure 7 the wing-drag coefficients of the tested wings are plotted against Mach number for a comparison of wings of two aspect ratios. The wings of aspect ratio 4 had less drag below $M \approx 1.2$, but greater drag above $M \approx 1.2$, than the wings of aspect ratio 2.

Figure 8 shows comparisons between the experimental and calculated wing-drag coefficients for each test configuration. The calculated results were obtained from the theory of references 1 and 2 and these results include a constant friction drag coefficient of 0.006. The theory has been applied to the present tests by assuming the body to form infinite end plates at the wing root. The agreement between the experimental and calculated results is quite good except for the two wings of aspect ratio 4, taper ratios 1/3 and 2/3. The theory qualitatively shows the same effect of taper and of aspect ratio as that shown by experiment.

CONCLUSIONS

An experimental investigation has been made of wing drag for swept-back tapered wings at zero lift with thin, symmetrical, double-wedge sections with free-stream profiles of 6-percent-thickness ratio. The midchord line of the wings was swept back 50°. The taper ratios tested were 0, 1/3, and 2/3, for aspect ratios, based on the exposed surfaces, of 2.0 and 4.0. The Mach number range of the tests was from $M = 1.0$ to 1.8.

Within the limits of the tests the results show that:

1. From $M \approx 1.0$ to $M \approx 1.3$, the wings with more taper give higher drag coefficients and, above a Mach number of 1.3, the wings with more taper show lower values of drag coefficient.

2. The wings of aspect ratio 4 had less drag below $M \approx 1.2$, but greater drag above $M \approx 1.2$, than the wings of aspect ratio 2.

3. In general, the experimental results yielded good agreement with the theory of NACA TN 1448 and TN 1672. The theory qualitatively shows the same effect of taper and of aspect ratio as that shown by experiment.

Langley Aeronautical Laboratory,
National Advisory Committee for Aeronautics,
Langley Field, Va., July 5, 1950.

REFERENCES

1. Margolis, Kenneth: Supersonic Wave Drag of Sweptback Tapered Wings at Zero Lift. NACA TN 1448, 1947.

2. Margolis, Kenneth: Supersonic Wave Drag of Nonlifting Sweptback Tapered Wings With Mach Lines Behind the Line of Maximum Thickness. NACA TN 1672, 1948.

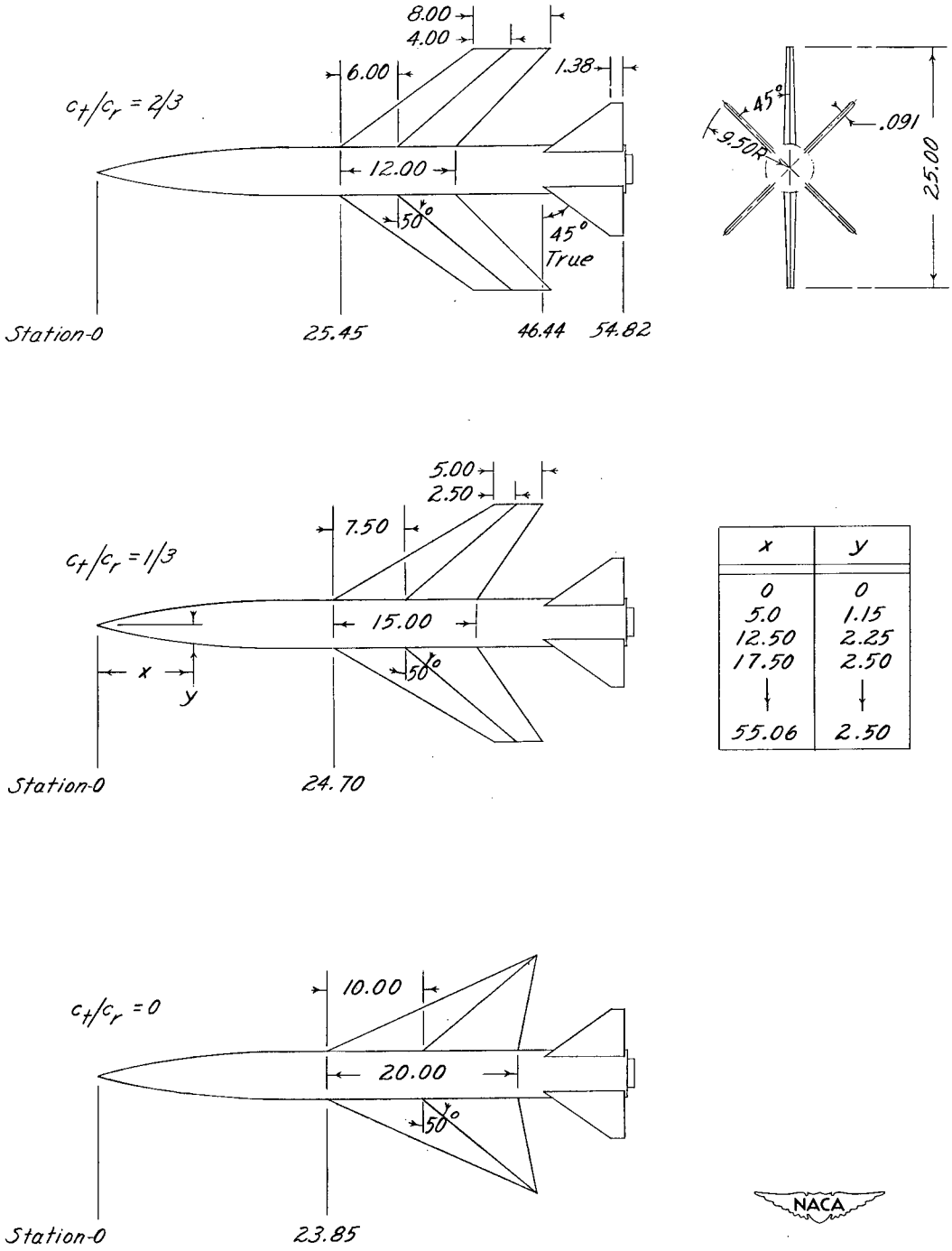

x	y
0	0
5.0	1.15
12.50	2.25
17.50	2.50
↓	↓
55.06	2.50

(a) Aspect ratio based on exposed surfaces, 2.0.

Figure 1.- Arrangement of test vehicles. Wing area (exposed), 200 square inches; fin area (4 fins exposed), 136.5 square inches.

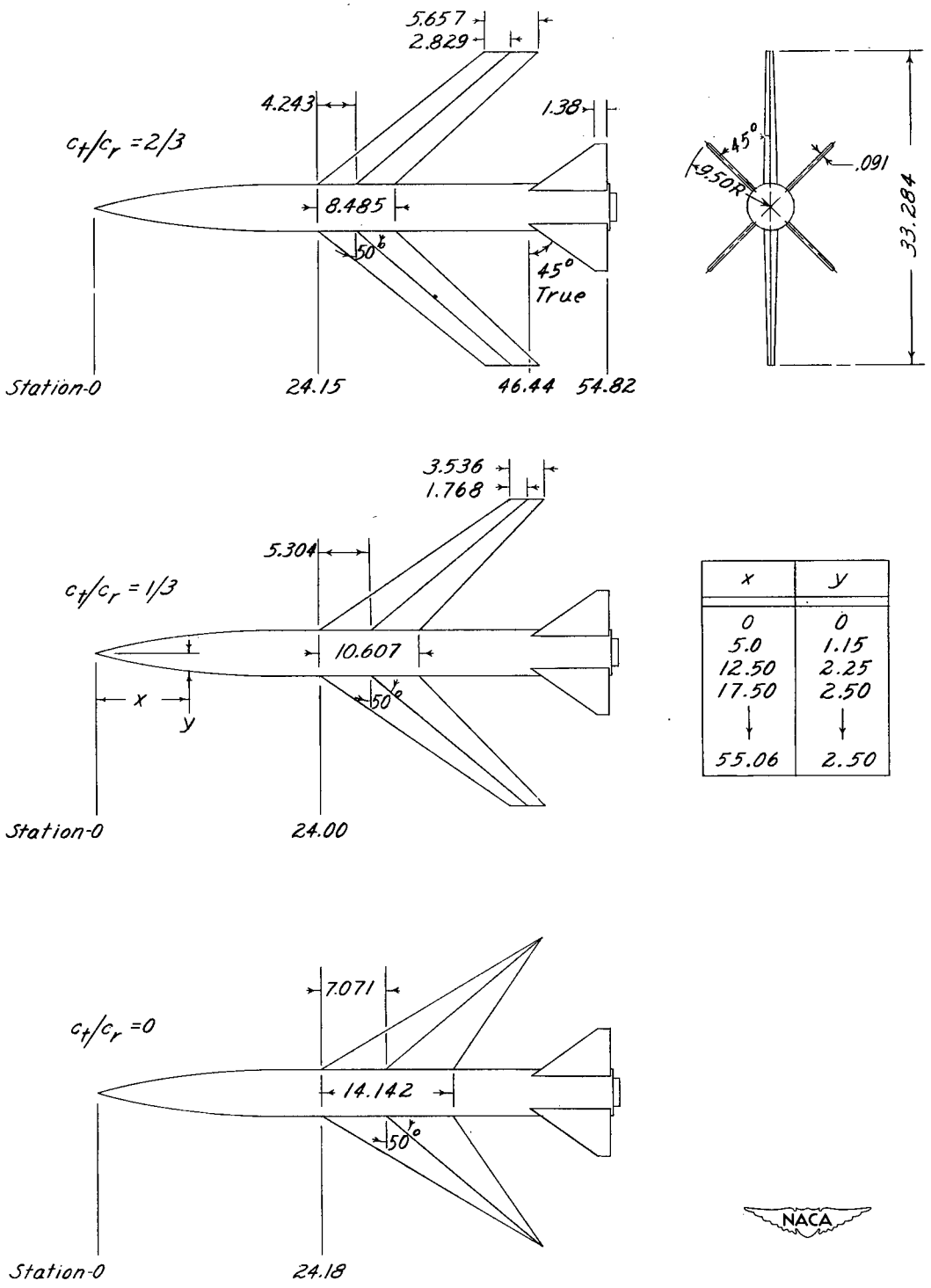

x	y
0	0
5.0	1.15
12.50	2.25
17.50	2.50
↓	↓
55.06	2.50

(b) Aspect ratio based on exposed surfaces, 4.0.

Figure 1.- Concluded.

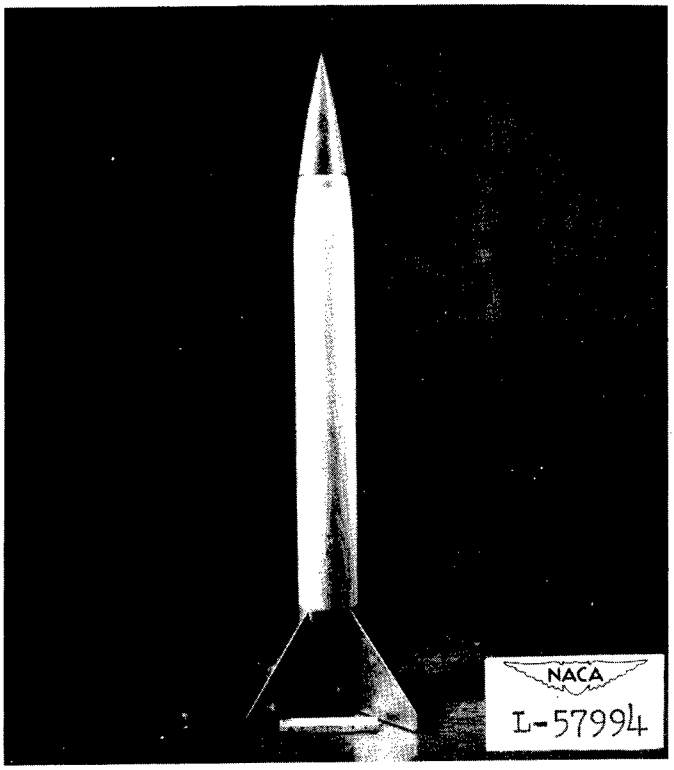

(a) Wingless body.

Figure 2.- Test vehicles.

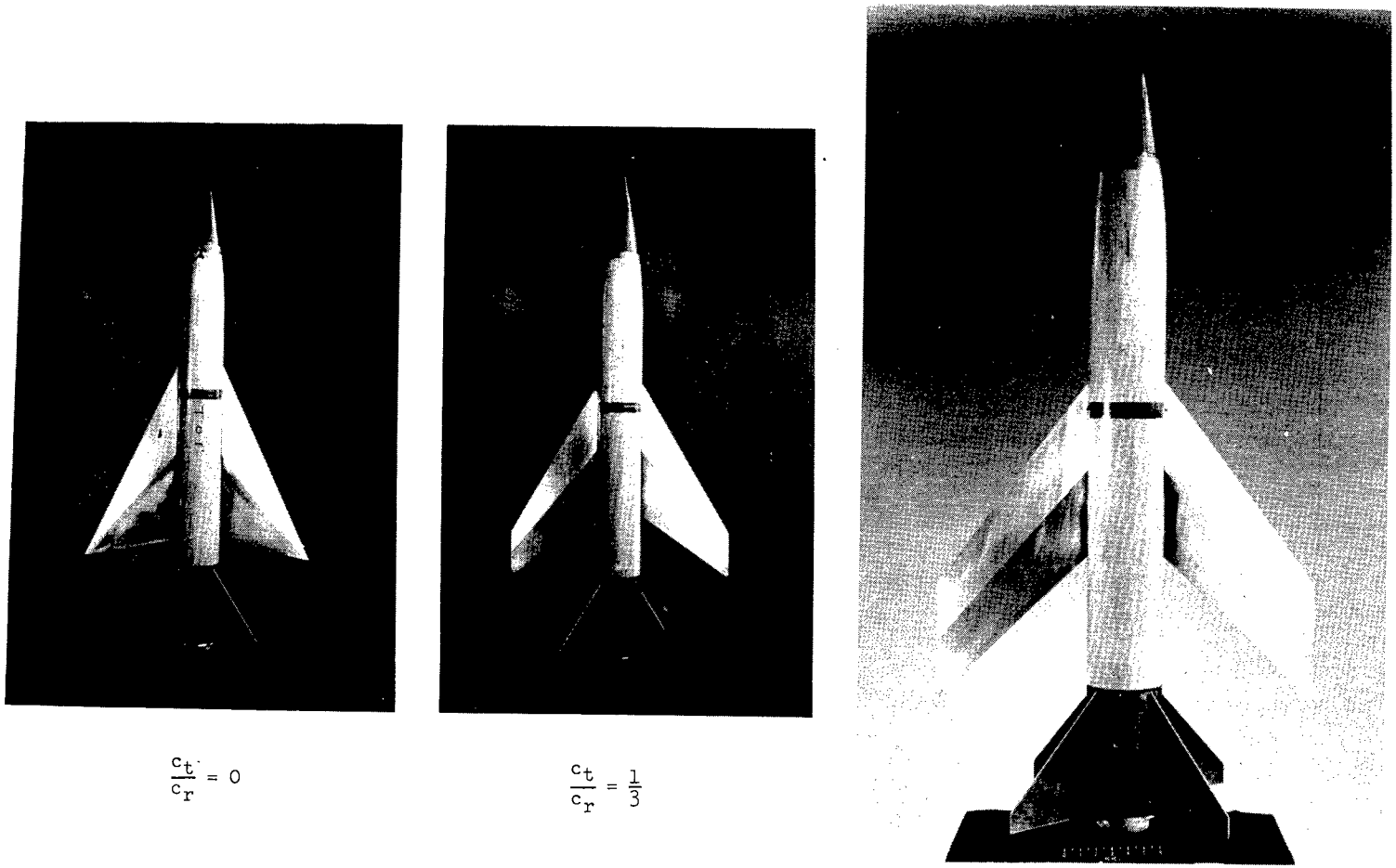

$\frac{c_t}{c_r} = 0$ $\frac{c_t}{c_r} = \frac{1}{3}$ $\frac{c_t}{c_r} = \frac{2}{3}$

NACA L-64909

(b) Bodies with wings of aspect ratio 2.0.

Figure 2.- Continued.

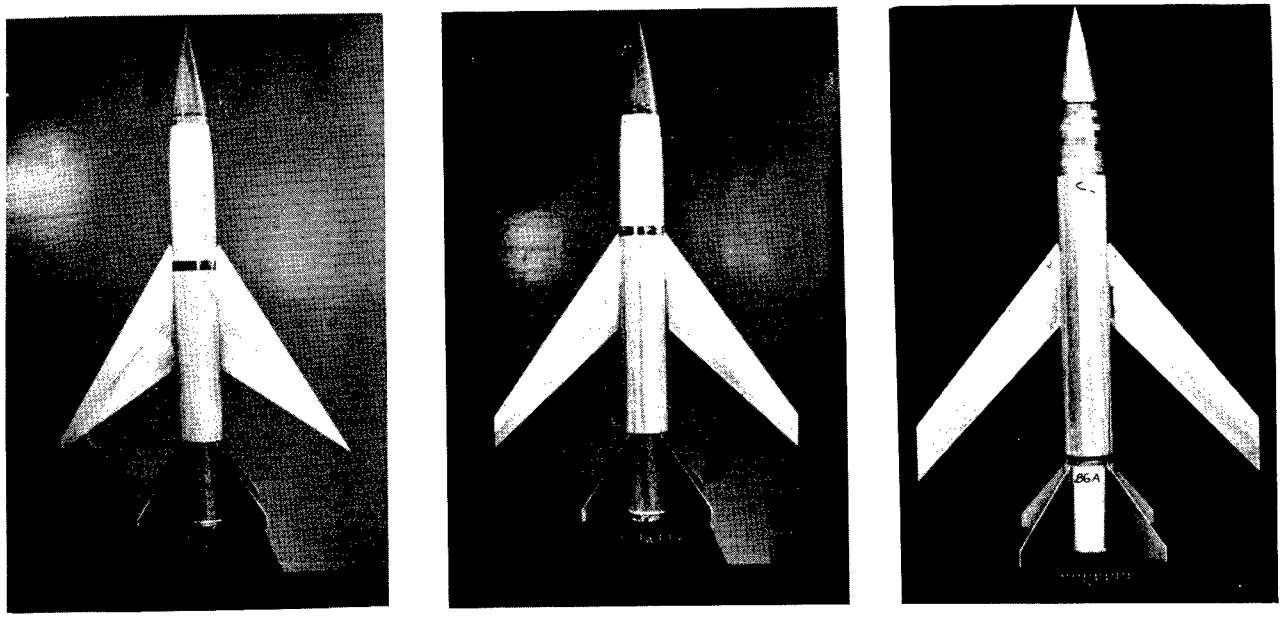

$\frac{c_t}{c_r} = 0$ $\frac{c_t}{c_r} = \frac{1}{3}$ $\frac{c_t}{c_r} = \frac{2}{3}$

NACA L-64910

(c) Bodies with wings of aspect ratio 4.0.

Figure 2.- Concluded.

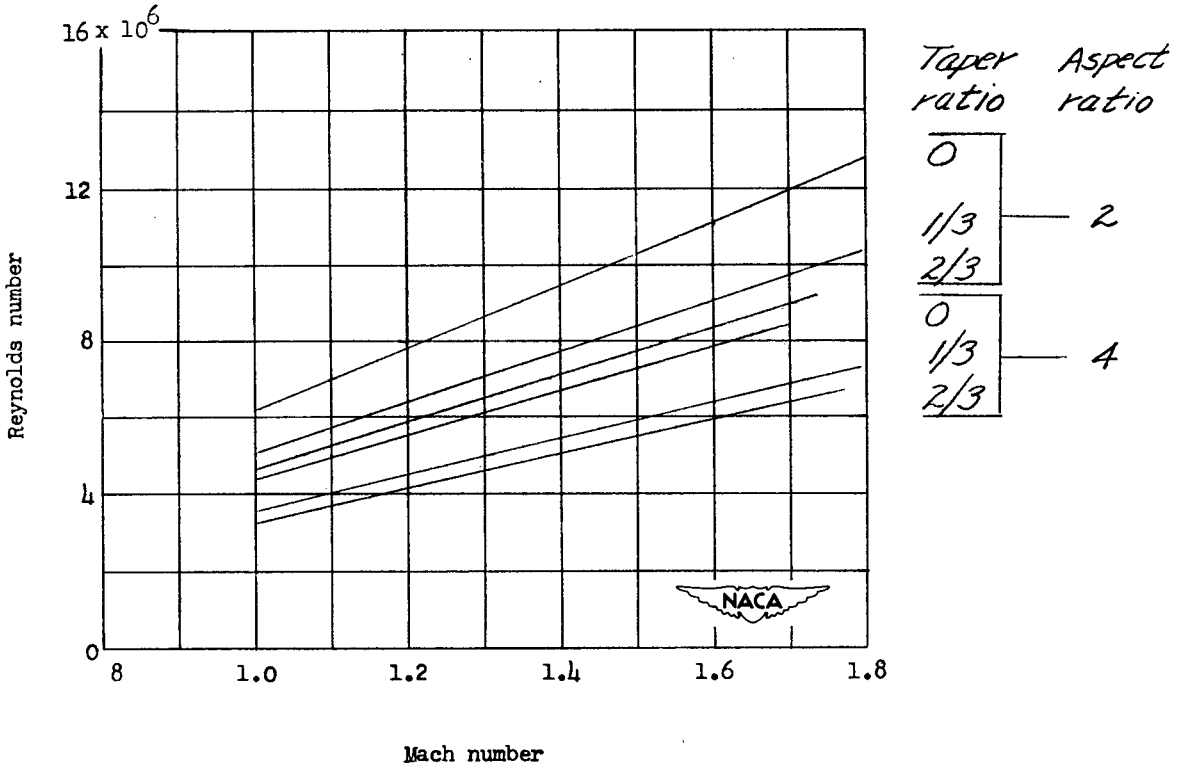

Figure 3.- Variation of Reynolds number with Mach number for each test configuration. Reynolds number based on mean aerodynamic chord of exposed wing surfaces.

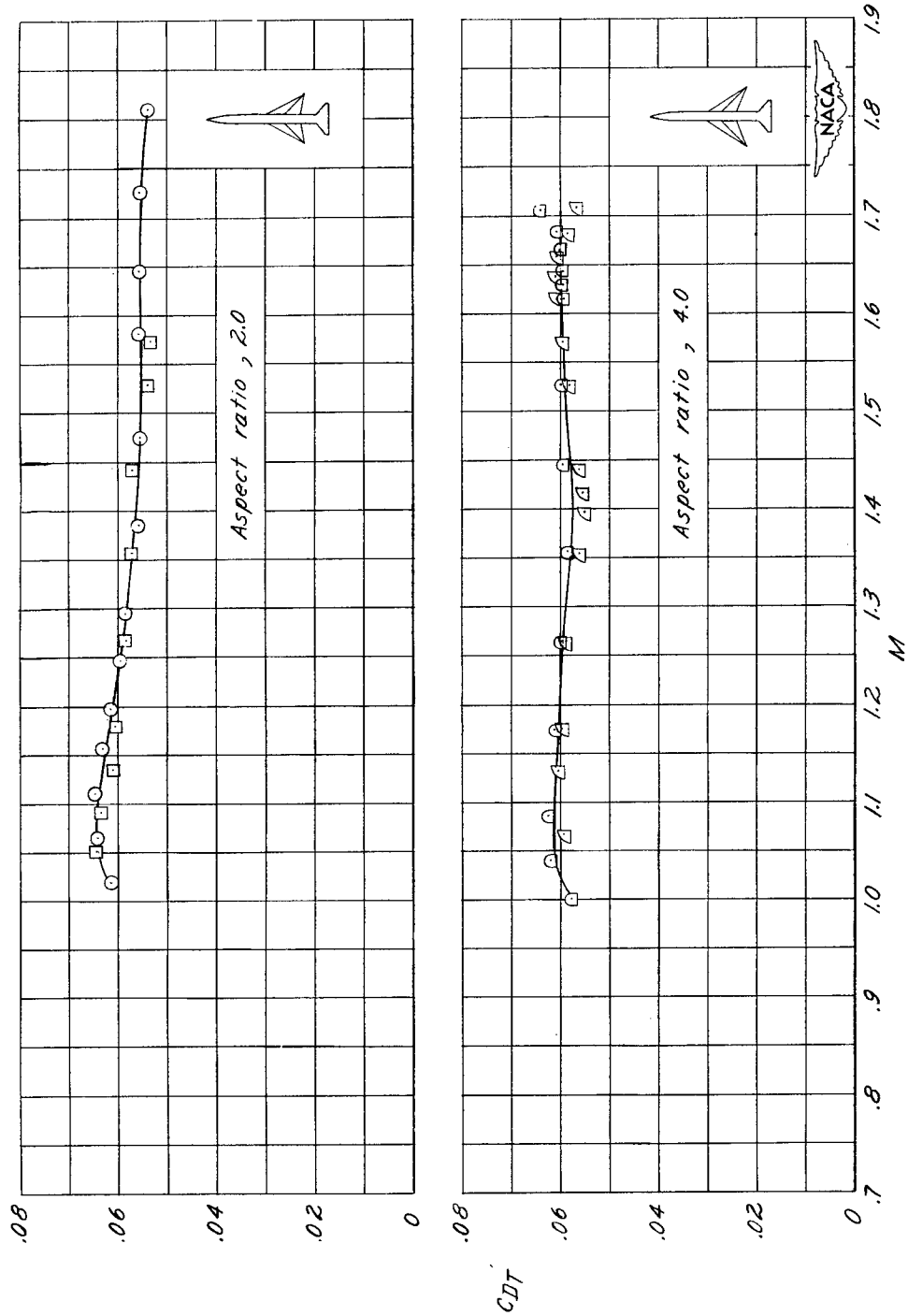

(a) Taper ratio, 0.

Figure 4.- Total-drag-coefficient data plotted against Mach number for the standard test body with wings for two aspect ratios based on an exposed wing area of 200 square inches.

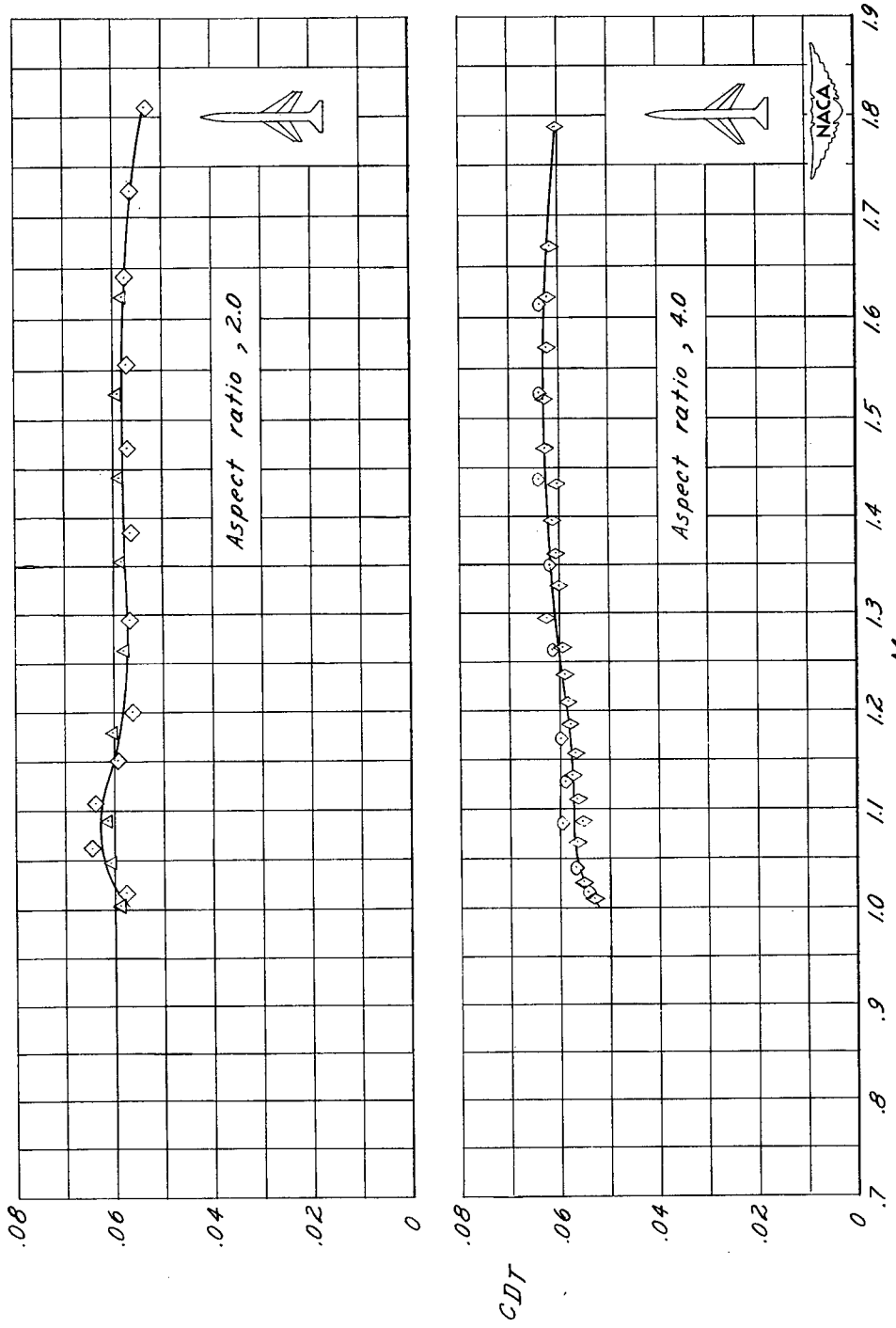

(b) Taper ratio, 1/3.

Figure 4.- Continued.

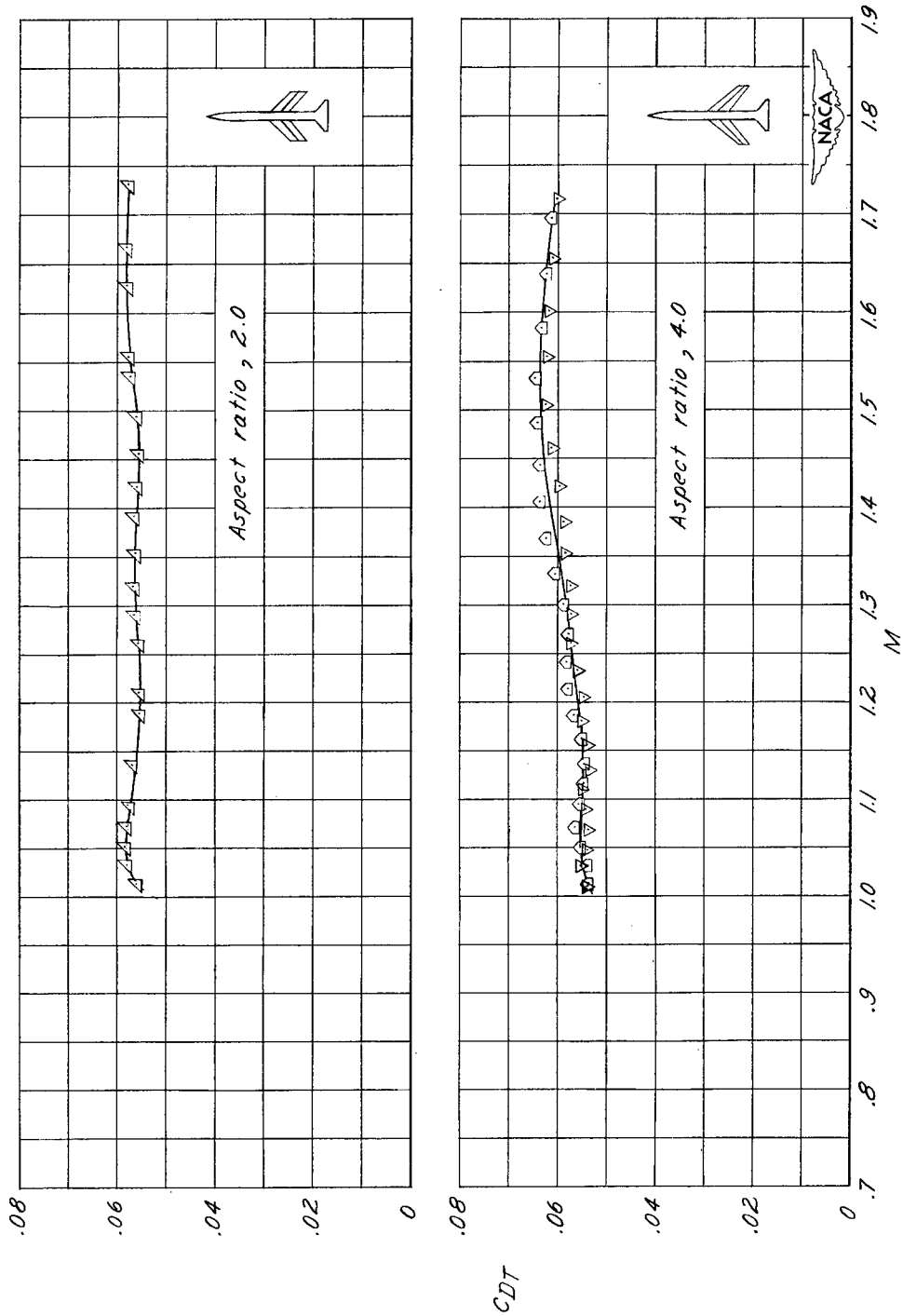

(c) Taper ratio, 2/3.

Figure 4.- Concluded.

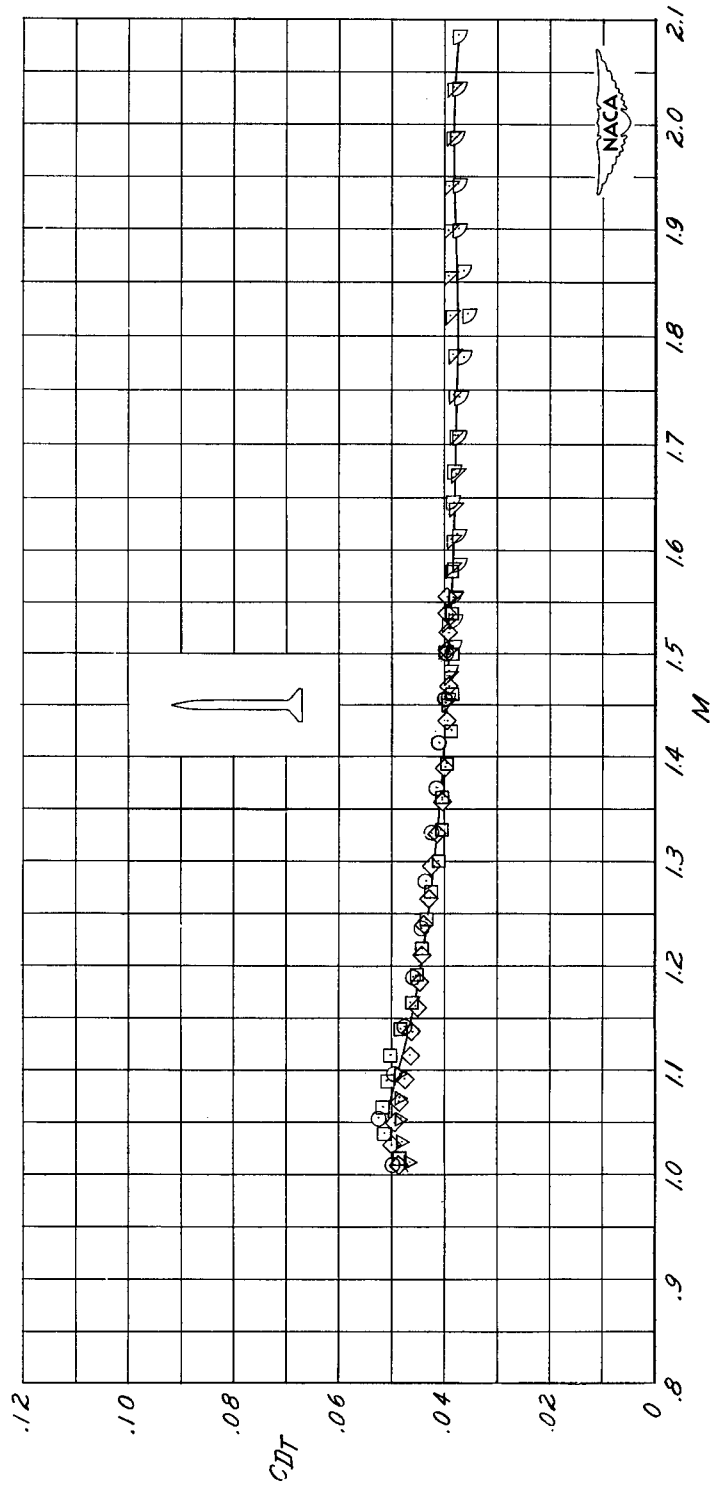

Figure 5.- Total-drag-coefficient data plotted against Mach number for six models of the standard test body less wings, based on exposed wing area of 200 square inches.

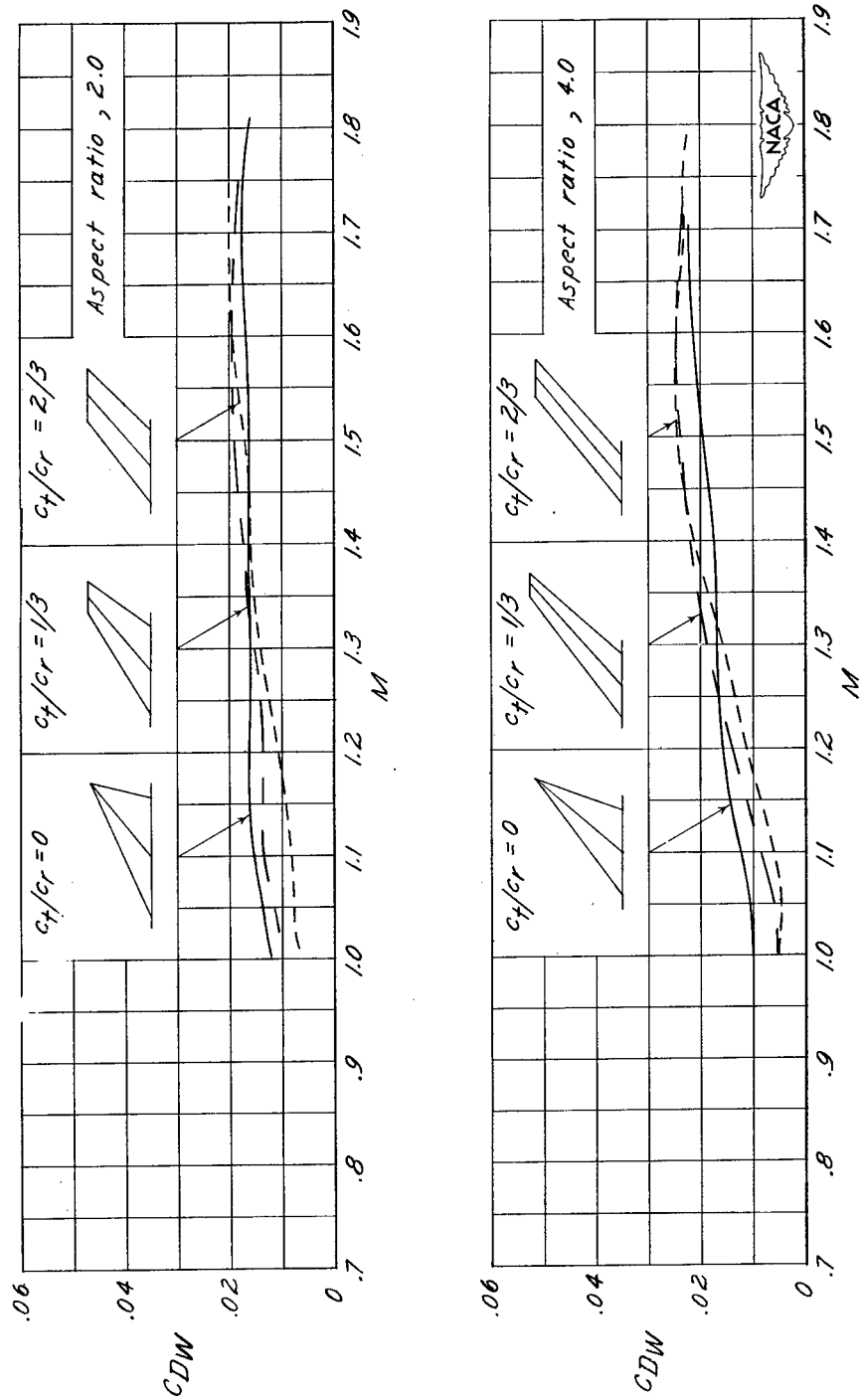

Figure 6.- Effect of taper ratio for wings of aspect ratio, based on exposed surfaces, of 4.0 and 2.0.

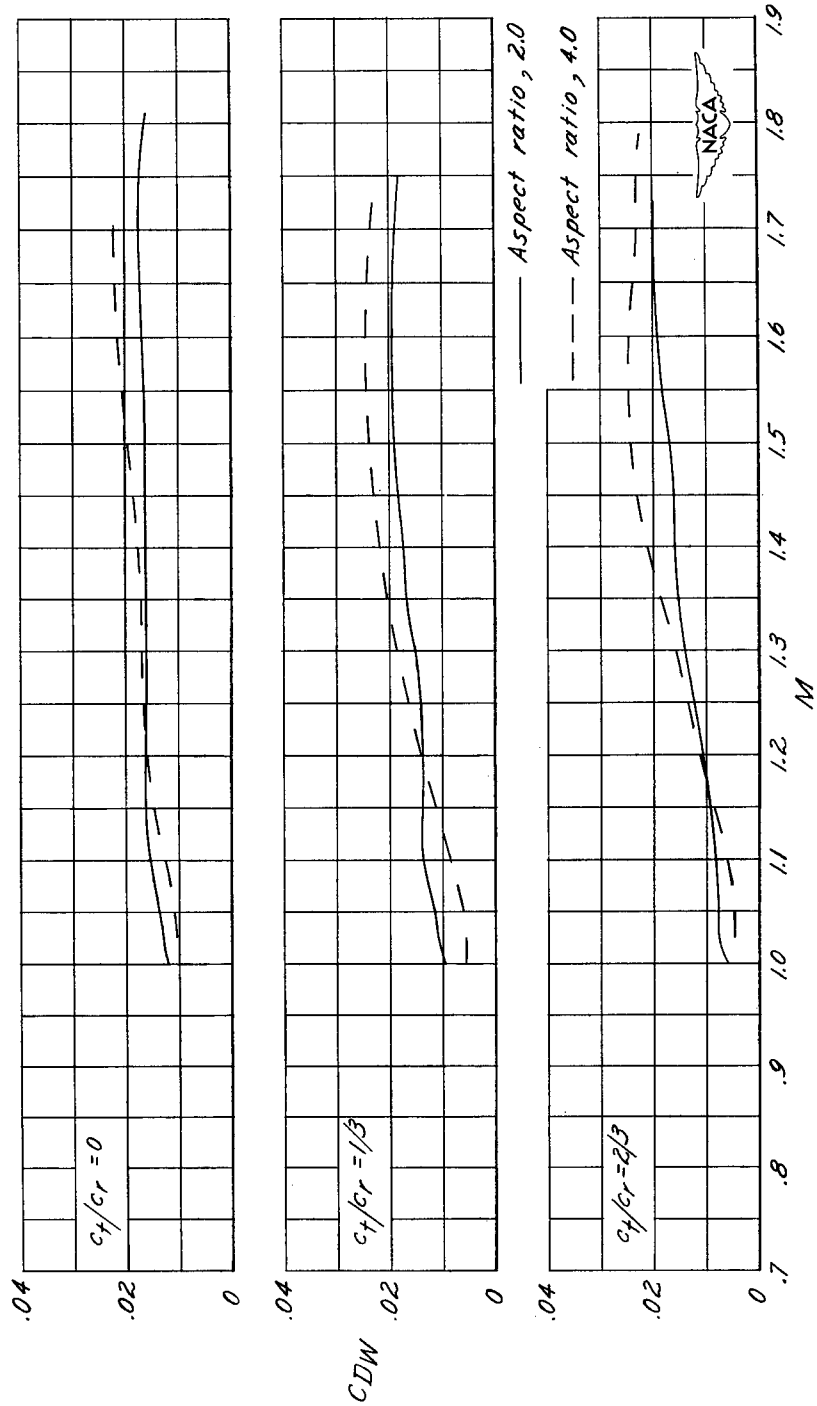

Figure 7.- Effect of aspect ratio for wings of three taper ratios.

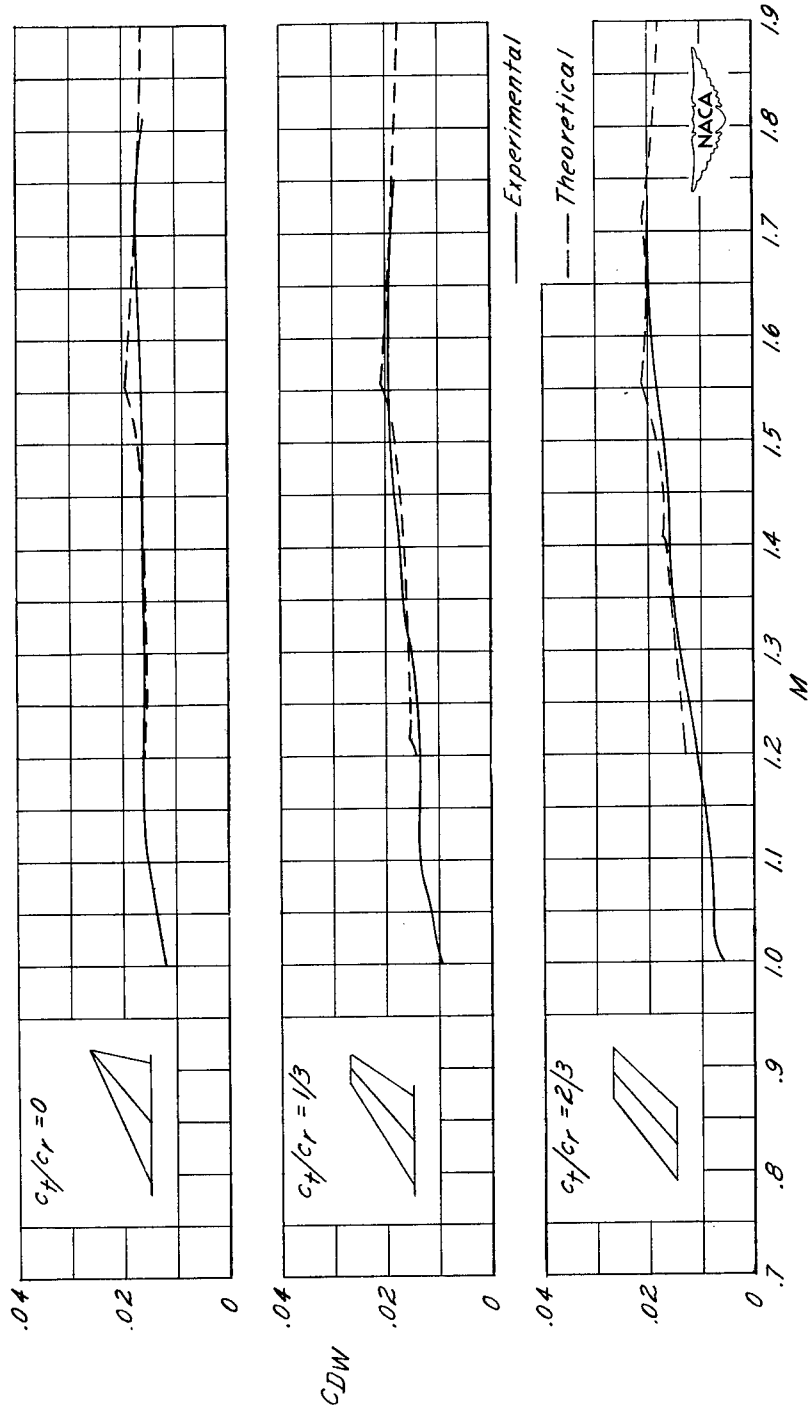

(a) Aspect ratio, based on exposed surfaces, 2.0.

Figure 8.- Comparison between experimental and theoretical wing-drag coefficients for three tapered wings.

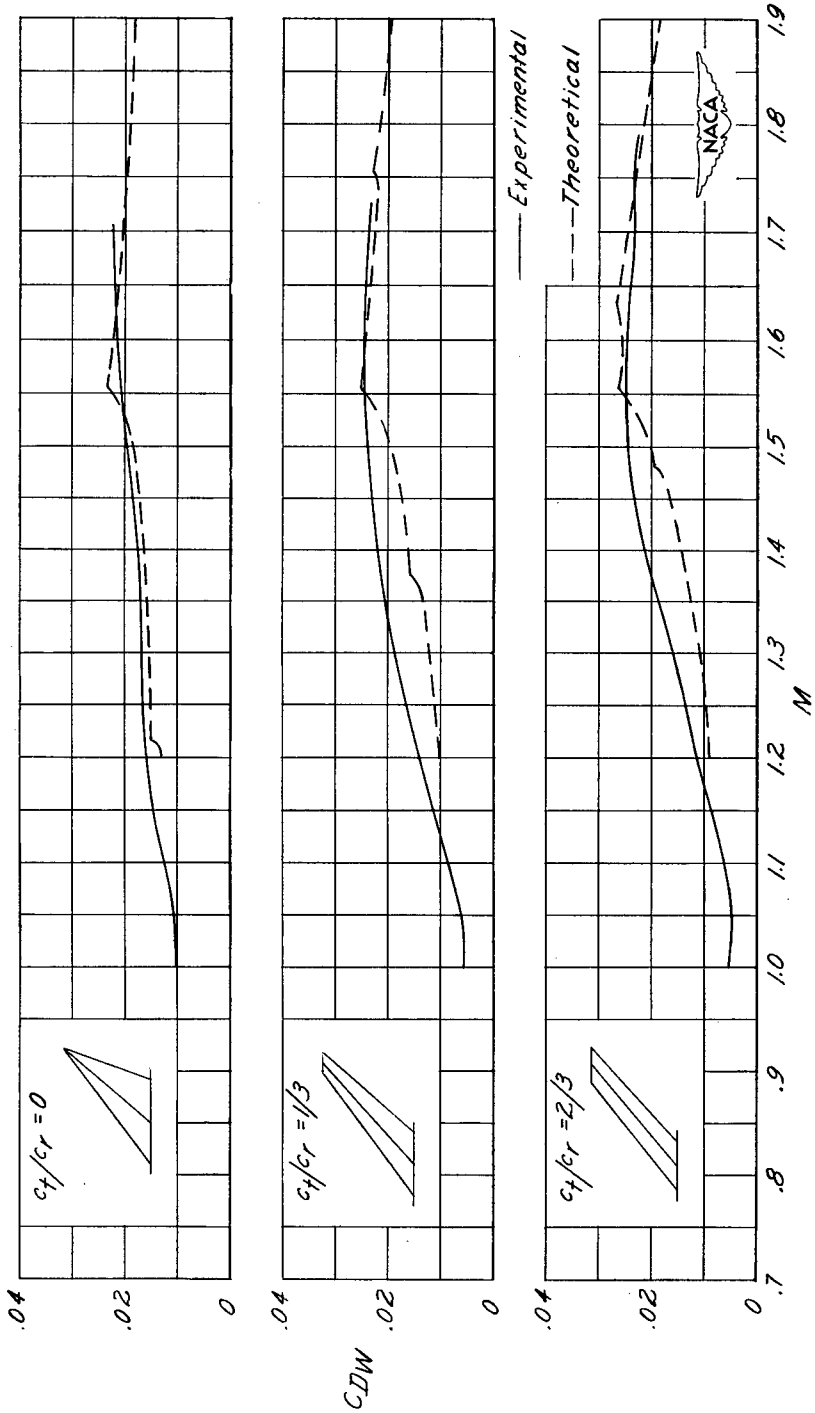

(b) Aspect ratio, based on exposed surfaces, 4.0.

Figure 8.- Concluded.

NACA TN 3697
National Advisory Committee for Aeronautics.
FLIGHT TESTS AT SUPERSONIC SPEEDS TO DETERMINE THE EFFECT OF TAPER ON THE ZERO-LIFT DRAG OF SWEPTBACK LOW-ASPECT-RATIO WINGS. Murray Pittel. June 1956. 20p. diagrs., photos. (NACA TN 3697. Supersedes RM L50F30a)

Comparison of experimental flight-test results with theoretical calculations to determine the effect of wing taper and aspect ratio on the zero-lift drag of wings with thin double-wedge sections at supersonic speeds is presented.

Copies obtainable from NACA, Washington

1. Wings, Complete - Theory (1.2.2.1)
2. Wings, Complete - Aspect Ratio (1.2.2.2.2)
3. Wings, Complete - Sweep (1.2.2.2.3)
4. Wings, Complete - Taper and Twist (1.2.2.2.4)
5. Mach Number Effects - Complete Wings (1.2.2.6)

I. Pittel, Murray
II. NACA TN 3697
III. NACA RM L50F30a

NACA TN 3697
National Advisory Committee for Aeronautics.
FLIGHT TESTS AT SUPERSONIC SPEEDS TO DETERMINE THE EFFECT OF TAPER ON THE ZERO-LIFT DRAG OF SWEPTBACK LOW-ASPECT-RATIO WINGS. Murray Pittel. June 1956. 20p. diagrs., photos. (NACA TN 3697. Supersedes RM L50F30a)

Comparison of experimental flight-test results with theoretical calculations to determine the effect of wing taper and aspect ratio on the zero-lift drag of wings with thin double-wedge sections at supersonic speeds is presented.

Copies obtainable from NACA, Washington

1. Wings, Complete - Theory (1.2.2.1)
2. Wings, Complete - Aspect Ratio (1.2.2.2.2)
3. Wings, Complete - Sweep (1.2.2.2.3)
4. Wings, Complete - Taper and Twist (1.2.2.2.4)
5. Mach Number Effects - Complete Wings (1.2.2.6)

I. Pittel, Murray
II. NACA TN 3697
III. NACA RM L50F30a

NACA TN 3697
National Advisory Committee for Aeronautics.
FLIGHT TESTS AT SUPERSONIC SPEEDS TO DETERMINE THE EFFECT OF TAPER ON THE ZERO-LIFT DRAG OF SWEPTBACK LOW-ASPECT-RATIO WINGS. Murray Pittel. June 1956. 20p. diagrs., photos. (NACA TN 3697. Supersedes RM L50F30a)

Comparison of experimental flight-test results with theoretical calculations to determine the effect of wing taper and aspect ratio on the zero-lift drag of wings with thin double-wedge sections at supersonic speeds is presented.

Copies obtainable from NACA, Washington

1. Wings, Complete - Theory (1.2.2.1)
2. Wings, Complete - Aspect Ratio (1.2.2.2.2)
3. Wings, Complete - Sweep (1.2.2.2.3)
4. Wings, Complete - Taper and Twist (1.2.2.2.4)
5. Mach Number Effects - Complete Wings (1.2.2.6)

I. Pittel, Murray
II. NACA TN 3697
III. NACA RM L50F30a

NACA TN 3697
National Advisory Committee for Aeronautics.
FLIGHT TESTS AT SUPERSONIC SPEEDS TO DETERMINE THE EFFECT OF TAPER ON THE ZERO-LIFT DRAG OF SWEPTBACK LOW-ASPECT-RATIO WINGS. Murray Pittel. June 1956. 20p. diagrs., photos. (NACA TN 3697. Supersedes RM L50F30a)

Comparison of experimental flight-test results with theoretical calculations to determine the effect of wing taper and aspect ratio on the zero-lift drag of wings with thin double-wedge sections at supersonic speeds is presented.

Copies obtainable from NACA, Washington

1. Wings, Complete - Theory (1.2.2.1)
2. Wings, Complete - Aspect Ratio (1.2.2.2.2)
3. Wings, Complete - Sweep (1.2.2.2.3)
4. Wings, Complete - Taper and Twist (1.2.2.2.4)
5. Mach Number Effects - Complete Wings (1.2.2.6)

I. Pittel, Murray
II. NACA TN 3697
III. NACA RM L50F30a